

# Self-Adhesive Silicone Microstructures for the Treatment of Tympanic Membrane Perforations

Gabriela Moreira Lana, Katharina Sorg, Gentiana Ioana Wenzel, Dietmar Hecker, René Hensel, Bernhard Schick, Klaus Kruttwig, and Eduard Arzt\*

Inspired by the gecko foot, polymeric microstructures have demonstrated reliable dry adhesion to both stiff objects and sensitive surfaces such as skin. Microstructured silicone patches are proposed, herein, for the treatment of tympanic membrane perforations with the aim of serving as an alternative for current surgical procedures that require anesthesia and ear canal packing. Sylgard 184 PDMS micropillars of 20  $\mu\text{m}$  in diameter and 60  $\mu\text{m}$  in length are topped by a Soft Skin Adhesive (SSA) MG7-1010 terminal layer, of about 25  $\mu\text{m}$  thickness. The adhesion is evaluated by specially designed tack tests against explanted murine eardrums and, for comparison, against a rigid substrate. Functional effects are evaluated using auditory brainstem responses (ABRs) and distortion product otoacoustic emissions (DPOAE). The adhesion strength of the microstructure and unstructured controls to explanted murine tympanic membranes is comparable (typically 12 kPa), but the microstructured patches are easier to handle by the surgeon. For the first time, partial recovery of hearing performance is measured immediately after patch application. The novel patches adhere without the need for further fixation, removing the need for ear canal packing. The proposed material design holds great promise for improving clinical treatments of tympanic membrane perforations.

## 1. Introduction

Micropatterning of polymeric materials is a powerful sustainable strategy for enhancing adhesion without the use of chemicals.<sup>[1]</sup> Such self-adhesive structures allow gentle and reversible adhesion in industrial robotics applications<sup>[2]</sup> and have been proposed for improved adhesive contact to human skin.<sup>[3–5]</sup> The principle is derived from the attachment organs of geckos, which can reversibly attach to vertical walls and ceilings.<sup>[6–9]</sup> Their adhesion is based on van der Waals interaction strongly enhanced by a compliant microfibrillar (“hairy”) structure. The main advantage of such dry adhesives lies in their chemical-free adhesive function, which would allow biomedical application without the need for further attachment agents.


Our research has focused on developing microstructured adhesives specifically for contact with human skin. Depending on many factors, e.g., location, age, and strain, skin can exhibit different roughness features.

Trojahn and coauthors measured in four different skin areas,  $R_a$  ranging from 13.9 to 16.2  $\mu\text{m}$  and  $R_z$  from 61.5 to 71.9  $\mu\text{m}$  (where  $R_a$  is the arithmetic mean deviation from the center line and  $R_z$  is the mean roughness depth).<sup>[10,11]</sup> Roughness is the main factor reducing adhesion due to insufficient molecular contact between the surfaces.<sup>[12]</sup> To achieve good adhesion under these circumstances, several materials strategies are available: 1) the dimensions of elastomeric micropillars can be chosen to optimize adhesion to a specific roughness;<sup>[13]</sup> 2) a compliant polymer film, when thinner than a critical thickness, can sufficiently conform to the surface irregularities to create reliable adhesion;<sup>[14]</sup> and 3) composite micropillars with very soft terminal layers can accommodate roughness of the countersurface.<sup>[8]</sup> Strategies (2) and (3) can be combined by designing a film-terminated structure in which arrays of micropillars are bridged at their terminal ends by a continuous compliant top layer. The mechanics of such film-terminated designs was discussed in detail by Glassmaker et al.<sup>[15]</sup> and Noderer et al.,<sup>[16]</sup> who attributed their superior adhesion to a crack-trapping mechanism: the interfacial crack “feels” the spatial modulation of the local compliance and is pinned in the space between the pillars, where the energy release rate to drive crack propagation is reduced. Such a microstructure can additionally adhere to

G. Moreira Lana, Dr. R. Hensel, Dr. K. Kruttwig, Prof. E. Arzt  
INM – Leibniz Institute for New Materials  
Campus D2 2, Saarbrücken 66123, Germany  
E-mail: eduard.arzt@leibniz-inm.de

G. Moreira Lana, Prof. E. Arzt  
Department of Materials Science and Engineering  
Saarland University  
Campus D2 2, Saarbrücken 66123, Germany

K. Sorg, Prof. G. I. Wenzel, Dr. D. Hecker, Prof. B. Schick  
Department of Otorhinolaryngology  
Saarland University Medical Center  
Homburg 66421, Germany

 The ORCID identification number(s) for the author(s) of this article can be found under <https://doi.org/10.1002/anbr.202100057>.

© 2021 The Authors. Advanced NanoBiomed Research published by Wiley-VCH GmbH. This is an open access article under the terms of the Creative Commons Attribution License, which permits use, distribution and reproduction in any medium, provided the original work is properly cited.

DOI: 10.1002/anbr.202100057

surfaces of different degrees of roughness<sup>[17]</sup> as the real contact area is increased due to the adaptation of the soft top layer and the compliant micropillars.<sup>[17–19]</sup>

The application proposed here for such microstructured films is the treatment of perforated tympanic membranes (TMs). Currently, tympanic membrane perforations (TMPs), especially in persistent or chronic cases, are treated by costly surgical procedures under anesthesia, involving the packing of the outer ear canal until the healing process is completed. This therapy impairs the patient's hearing and could implicate surgery complications.<sup>[20]</sup> Due to these risks of TMP treatments, biomaterials research started to look for promising therapeutic alternatives for TM regeneration, especially for the treatment of large or persistent perforations. Even when perforated membranes heal spontaneously, the repaired membranes can be malformed, acoustically suboptimal, and susceptible to re-perforations.<sup>[20]</sup> The time of healing and the closure rate of TMPs strongly depend on the type (acute or chronic) and size.<sup>[21,22]</sup> Recurring and chronic perforations can cause, in addition to hearing loss,<sup>[23–25]</sup> severe health issues due to the risk of infections and of cholesteatoma formation.<sup>[26]</sup> A fast and mechanically reliable closure of the perforation is therefore indicated.

The TM has an important role in sound transmission to the ossicles and in protecting the middle ear. By collecting vibrations from the incoming sound waves and transforming into mechanical waves as vibrations, the TM is an important factor of the acoustic impedance system. Disturbances in this mechanical system lead to hearing impairment. This can be quantified by recording the auditory brainstem response (ABR) and by measuring the distortion product otoacoustic emissions (DPOAEs). ABR signals generated in the auditory cortex can be detected by peripheral electrodes using a standard method for diagnostic purposes in humans and research purposes in laboratory animals, often along with DPOAEs.<sup>[27,28]</sup> The latter is an important frequency-specific method to detect the functional effects of middle ear disorders, such as otitis media, TMPs, and discontinuity of the ossicular chain.<sup>[29–31]</sup> DPOAE measurements are a very sensitive tool to analyze mechanical alterations in the middle ear, among other things, and therefore can also be used to obtain information about the healing process of the perforated tympanic membrane.<sup>[32]</sup>

In the clinic, acute clean TMPs that are not very large and present no other complications, e.g., large destruction of the edges or involvement of the ossicular chain, are treated by unrolling, subtle correction of their edges, and overlaying a film, which should protect the middle ear and support the healing process. For larger or persistent TMPs, a surgical procedure called myringoplasty, or tympanoplasty, is needed as was first described by Zöllner<sup>[33]</sup> and Wullstein.<sup>[34]</sup> An autologous film (perichondrium, cartilage, or fascia) is positioned underneath the perforation with freshly cleaned margins. For both medical treatments, the newly introduced material needs to be kept in position by packing the outer ear canal, e.g., with a layer of silicon stripes and finally with antibiotic-impregnated gel foam. As an alternative procedure, simple silicone foils can be used to sustain the healing process, reducing the risk of ear infections and possibly improving hearing abilities for small and medium TMPs.<sup>[35,36]</sup> In a clinical study, polydimethylsiloxane (PDMS) films, in combination with immobilized collagen, were used to treat small TMPs with a

success rate of 70%.<sup>[37]</sup> We previously proposed the soft skin adhesive SSA MG7-9800 for this purpose due to its reliable but gentle self-adhesion to tissues, enabling secure adherence and atraumatic removal.<sup>[38,39]</sup> Patching perforated eardrums with self-adhesive materials in humans could therefore improve the treatment for the affected patients and has however, to our knowledge, not been reported so far.

We designed a novel self-adhesive patch in the form of film-terminated microstructured silicone film. For the micropillars, PDMS Sylgard 184 was chosen, whereas the top layer consisted of a soft skin adhesive (SSA MG7-1010). The patches were evaluated, in comparison to nonstructured control samples, regarding adhesion to rigid rough substrates and to explanted murine eardrums. In addition, the functional properties for restoring hearing after closing of TMPs by the adhesive patches were evaluated by click ABR and DPOAE measurements. The resulting properties of the novel patch were extremely encouraging and suggest finalizing the preparations for clinical studies.

## 2. Results

### 2.1. Film-Terminated Microstructured and Control Samples

Film-terminated microstructures consist of a pillar array microstructure topped by a soft skin adhesive layer. Pillars were fabricated by replica molding of Sylgard 184 and subsequently integrated to the SSA layer. **Figure 1a** shows the film-terminated microstructured architecture is schematically illustrated. The scanning electron micrograph presented in **Figure 1b** shows that the actual aspect ratio of the pillars supporting the top layer was somewhat smaller than the designed value 3 because the dipping process required for integration of the MG7-1010 top had created some overlap. Among all sets fabricated, thickness values of the film-terminated microstructures were  $43.2 \pm 1.9 \mu\text{m}$  for the backing layer,  $44.7 \pm 3.0 \mu\text{m}$  for the micropillars, and  $24.9 \pm 3.3 \mu\text{m}$  for the top layer, in total,  $\approx 112 \mu\text{m}$  (**Figure 1c**). The unstructured controls consisted of a  $58.9 \pm 2.3 \mu\text{m}$ -thick Sylgard 184 layer and a  $24.1 \pm 1.9 \mu\text{m}$ -thick MG7-1010 top layer, with a total thickness of  $\approx 85 \mu\text{m}$ . The mass per area was  $\approx 0.08 \text{ mg mm}^{-2}$  for the two specimen types.

### 2.2. Roughness

To define the roughness of the murine tympanic membrane, replicas were produced by imprinting with a room-temperature fast-curing silicone, applied through the outer ear canal on the exposed tympanic membrane. Subsequently, the roughness was determined from the silicone replicas using confocal scanning microscopy. The arithmetic mean height ( $R_a$ ) of the replicas of explanted TMs was  $0.14 \pm 0.04 \mu\text{m}$ . In comparison, the arithmetic mean height ( $R_a$ ) of the epoxy substrate used in the adhesion measurements carried out in laboratory was  $0.41 \pm 0.01 \mu\text{m}$ . Mean peak to valley roughness ( $R_z$ ) values were  $1.18 \pm 0.42 \mu\text{m}$  for the TM replicas and  $2.5 \pm 0.08 \mu\text{m}$  for the epoxy substrate. Root mean square (RMS) roughness values were  $90 \pm 31$  and  $12 \pm 1 \mu\text{m}$ , respectively.

Exemplary surface scans of the TM replicas and the epoxy substrate are shown in **Figure 2**. The two measurements of the TM replicas (**Figure 2b,c**) show some differences, which illustrate the

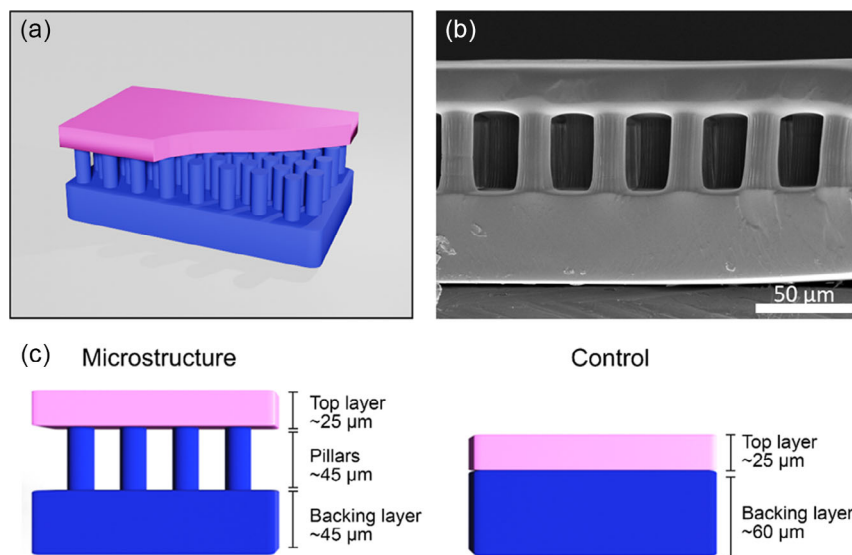


**Figure 1.** Film-terminated microstructure proposed for repair of tympanic membranes. a) 3D representation of the film-terminated design, Sylgard 184 in blue and soft skin adhesive SSA MG7-1010 in pink. b) Scanning electron micrograph of an actual microstructure, side view. c) Schematic illustration showing the approximate dimensions of the top layer, pillar portion, and backing layer for film-terminated samples in contrast to the top layer and backing layer in the unstructured control sample.

large deviation between different measurements and will reflect on deviations in adhesion measurements, described later. The scan of the epoxy substrate is shown in Figure 2d.

### 2.3. Pull-Off Stress Against Epoxy

First, the adhesion of the microstructured and control patches was measured against the rigid epoxy substrate of roughness  $R_z$  of 2.5  $\mu\text{m}$ . **Figure 3** shows that the microstructured adhesive had a significantly higher adhesion to epoxy than the unstructured control sample: after applying a compressive prestress of 11 kPa, the microstructures detached at  $72.7 \pm 9.4$  kPa and the control samples at  $39.4 \pm 16.5$  kPa; the improvement factor was 1.89 ( $p$ -value 0.001). For a prestress of 23 kPa, the microstructures exhibit similar adhesion values, but the improvement factor went down to 1.27 ( $p$ -value 0.03). This was due to the strong increase in the unstructured control samples by 56 % at the higher prestress, presumably due to better conformation to the substrate roughness.

### 2.4. Adhesive Strength Against Murine TMs Using Ex Vivo Tests

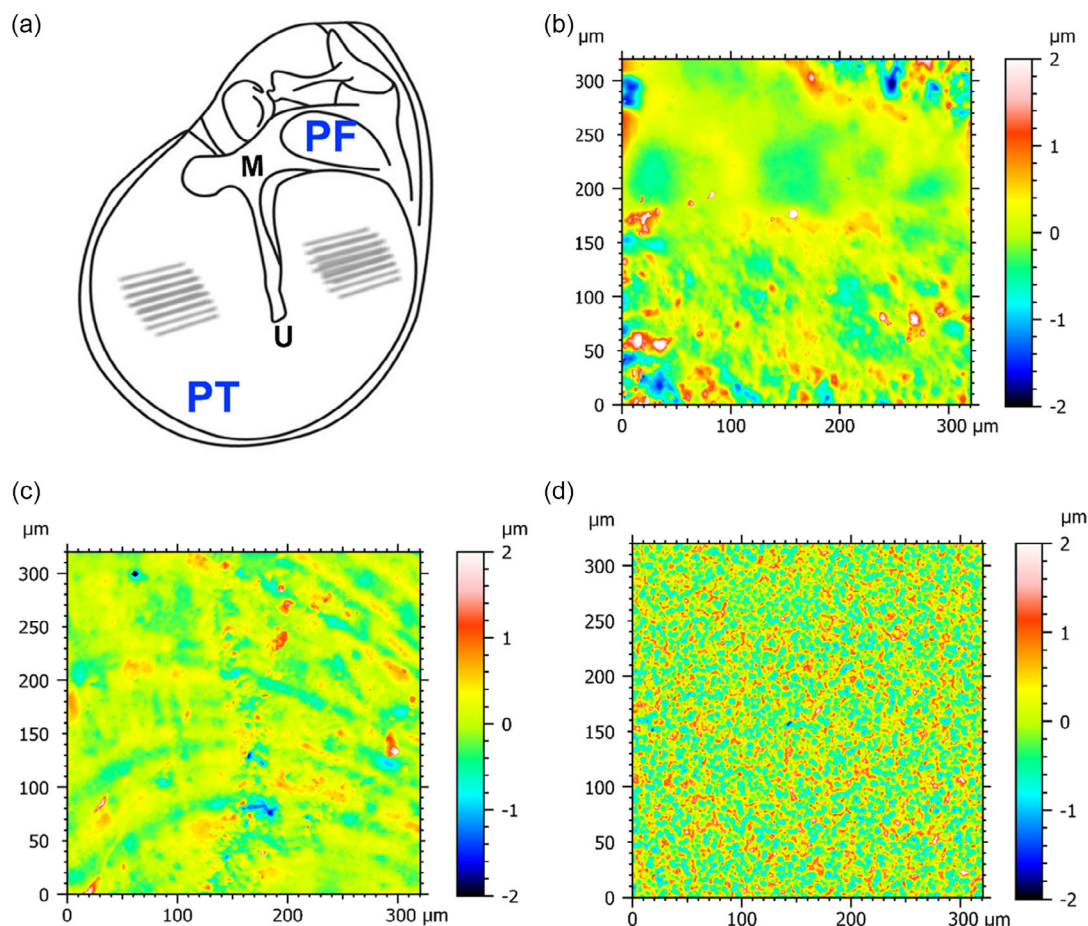
To evaluate the adhesion of the patches closer to real conditions, adhesion measurements were carried out on intact and perforated, explanted tympanic membranes of mice, **Figure 4a** shows an explanted murine petrosal bone with the TM exposed. Three different adhesive patches were tested: 1) film-terminated microstructures, 2) control films with its adhesive side (MG7-1010 layer) adhered to the TM, and 3) control films with nonadhesive backside (Sylgard 184 layer). The custom-made sample holder was used to align the explanted TM in a 90° angle to the patch applicator, as shown in Figure 4b,c. As shown in

Figure 4a, the patches were positioned to fully cover the perforation. Care was taken that the patch had still enough overlap with the remaining membrane to ensure its adhesion. The size of an average perforation was about  $700 \times 500 \mu\text{m}^2$ ; this amounted to roughly 10% of the total area of the murine tympanic membrane (with typical dimensions of  $2 \times 2 \text{ mm}^2$ ) and  $\approx 40\%$  of the patch area (1 mm diameter).

Exemplary stress versus time curves (Figure 4d) for measurements on intact (blue) and perforated (green) TMs demonstrate the gradual increase in the compressive prestress up to a set value of  $\approx 25$  kPa. To conduct the experiments in the shortest time possible and avoid therefore changing in the membrane's properties, we limited the compressive preload condition to one value. The position was held for 10 s, which was accompanied by some slight relaxation possibly due to the soft top layer. Upon retraction, patches detached at various tensile loads. The detachment is typical for tack measurements of soft materials.<sup>[40]</sup>

Our results on intact TMs (**Figure 5a**) demonstrated that the adhesive strength of the film-terminated microstructure patches was significantly higher compared with the nonadhesive, unstructured control ( $p = 0.002$ ) but not higher than the adhesive side of the control sample. The mean pull-off stress of microstructured patches was  $14.5 \pm 8.8$  kPa, with a maximum of 32.3 kPa and a minimum of 5.7 kPa. Mean value for the adhesive control was  $13.3 \pm 7.2$  and  $5.7 \pm 4.6$  kPa for the nonadhesive control. The mean pull-off stress of the film-terminated microstructured patches was  $\approx 9\%$  higher, but not statistically significant, compared with the adhesive control ( $p = 1$ ). An explanation for the large deviation probably relates to large variations of the explanted TMs and the conditions of the ex situ adhesion measurements.

On the perforated TM (Figure 5b), the pull-off stress values were overall reduced compared with the intact condition. In



**Figure 2.** Surface roughness of murine TMs and epoxy substrate. a) Measurement locations in the pars tensa (PT), which is separated by the malleus (M) with its lowest part at the umbo (U). PF is pars flaccida. b,c) Inverse topography scans of tympanic membrane measured on silicone replicas. d): Topography scan of the epoxy substrate. Roughness measurements were obtained from 14 replicas of 7 TMs measured in three different positions of the PT, and for epoxy substrates in three independent positions.

the adhesive and nonadhesive control sample, adhesion decreased by 43% and 49%, which is comparable with the loss of contact area due to the perforation; by contrast, microstructured patches suffered only a 17% reduction. The adhesion of the film-terminated microstructure ( $p$ -value 0.002) and the adhesive, unstructured control ( $p$ -value 0.006) was significantly higher than the nonadhesive control. The difference between the microstructured adhesive patches and the adhesive control samples were higher than before (14.5–13.3 vs 12.1–7.6 kPa), but again not statistically significant ( $p = 0.14$ ).

## 2.5. Physiological Effects on the Hearing Performance

To gain information about the overall hearing function, ABR recordings were carried out as a standard method to determine auditory function in vivo. Thereby, the hearing threshold under three conditions was analyzed: 1) on intact TM; 2) perforated TM; and 3) after applying a patch on the perforation.

The results of the click ABR recordings demonstrated that the hearing threshold significantly increased after perforation from 12 dB SPL to 34 dB SPL in both groups, which translates into an

increase of 283% ( $p$ -value 0.003 and 0.01, respectively). Covering the perforation with patches led to a statistically nonsignificant decrease in the threshold in both groups with microstructured patches as well as unstructured control patches (Figure 6a,b).

The click-ABR is testing, however, the cumulative hearing activation overlapping the induced activation of all frequencies included in the click applied. The technique is therefore not sufficiently sensitive for judging the hearing improvement at individual frequencies through patch application. Therefore, to analyze the effects of closing the perforation in a more sensitive and frequency-specific manner, DPOAE recordings were carried out after ABR measurements. The results of the in vivo DPOAE measurements in anesthetized mice with intact and perforated TM were compared after the closure of the perforation with the two different patches, i) the film-terminated microstructured patch and ii) the unstructured adhesive control (Figure 7a,b). Through this, a difference between the lower frequencies (10–15 kHz) and the higher frequencies (15–18 kHz) could be measured.

The averaged DPOAEs between 10 and 15 kHz demonstrated an improvement after applying microstructured patches (Figure 7c). Here, the DPOAE signals dropped from



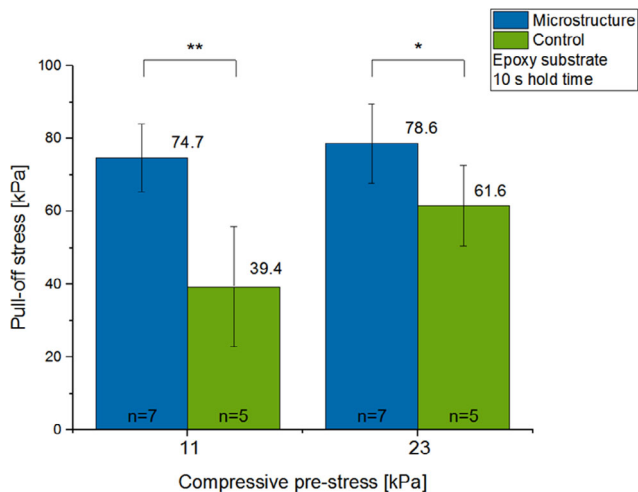


**Figure 3.** Adhesion of film-terminated microstructures and unstructured controls as determined by tack tests against epoxy substrates. The compressive prestress was varied from 11 (left) to 23 kPa (right). The hold time at prestress was 10 s. The data are presented as mean  $\pm$  SD. The mean values are labeled above each graph. Number of experiments: seven measurements for film-terminated microstructures and five measurements for control samples,  $p$ -values are calculated using two-sided  $t$  test. \* characterizes  $p < 0.05$  and \*\* indicates  $p < 0.01$ .

26.4  $\pm$  2.3 dB in intact condition, by  $\approx 34\%$ , to 17.5  $\pm$  3.8 dB after perforation ( $p = 1.27 \times 10^{-6}$ ). The application of film-terminated microstructure led to a highly significant increase to 21.8  $\pm$  2.9 dB (Figure 7c) corresponding to + 25 % ( $p = 0.006$ ). By contrast, in the group treated with control adhesives (Figure 7d), the same proportional decrease was followed by an increase by  $\approx 21\%$  to 21.2  $\pm$  4 dB, which is statistically not significant ( $p = 0.06$ ). In the higher-frequency range, from 15.5 to 18 kHz (Figure 7e,f), the DPOAE signals decreased after perforation by  $\approx 24\%$  from 30.1  $\pm$  3.3 to 23  $\pm$  2.8 dB for the microstructure and by  $\approx 28\%$  from 30.7  $\pm$  2.4 to 22.1  $\pm$  4.9 dB for the control group. The application of the film-terminated microstructure led to a non-significant improvement from 23 to 23.2 dB being  $\approx +0.7\%$  of the DPOAEs ( $p = 1$ ), whereas the application of control films led to a significant increase by about 10% from 22.1 to 24.5 dB ( $p = 0.02$ ). In none of these measurements, full recovery of the DPOAE levels to intact levels was achieved by patching in the acute herein presented conditions.

As mass and damping are essential parameters to be considered in analyzing the vibratory characteristics of a structure, we also investigated the effects of applying microstructured and control patches (in the thin and additionally coarser dimensions  $\approx 300 \mu\text{m}$  total thickness) on the intact membrane and gained more information on the influence of patching on the sound conduction

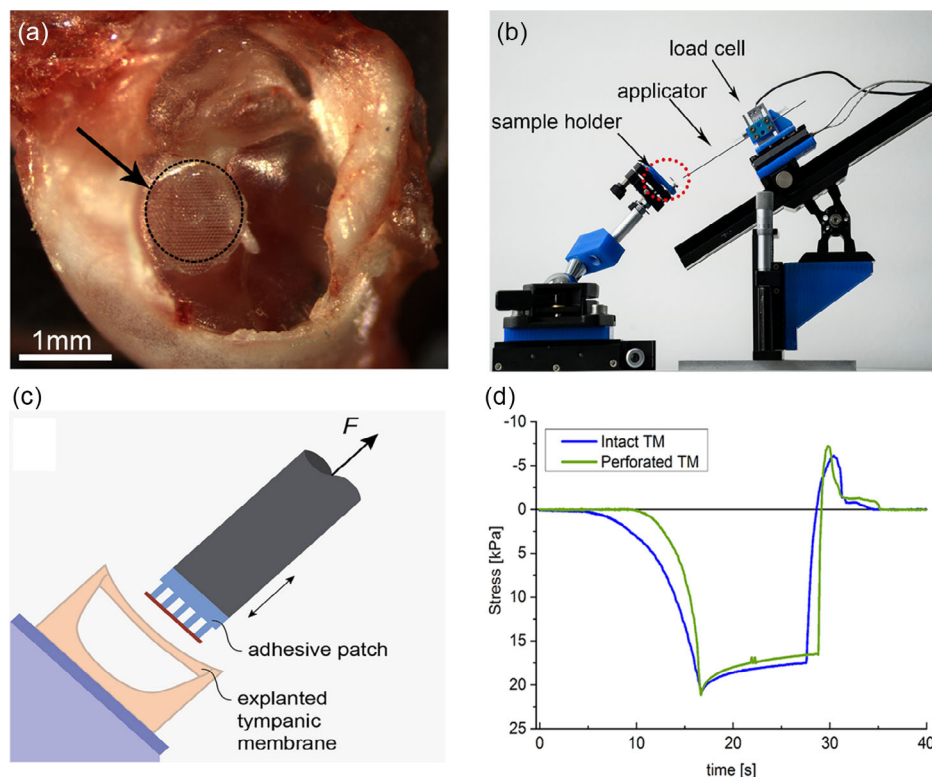


**Figure 4.** Ex vivo adhesion tests on intact and perforated murine TMs. a) Photograph of a film-terminated microstructured patch (indicated by the black arrow + dotted line) covering a perforation in the upper posterior quadrant of the murine TM. b) The measurement setup consisting of an adjustable sample holder to fix the explanted tympanic membrane and the adhesive patch mounted on a motorized applicator equipped with a load cell. c) Illustration of the test procedure indicated in b) as red dotted circle: TMs with petrosal bone mounted on a glass substrate was contacted by the adhesive patch, ensuring parallel contact. d) Exemplary stress versus time curve: The compressive prestress of  $\approx 25$  kPa was held for 10 s and the patch detached completely from the intact (blue line) or perforated (green line) TM at stresses of about 8 kPa. Positive values indicate compressive stress, and negative indicate tensile stress.

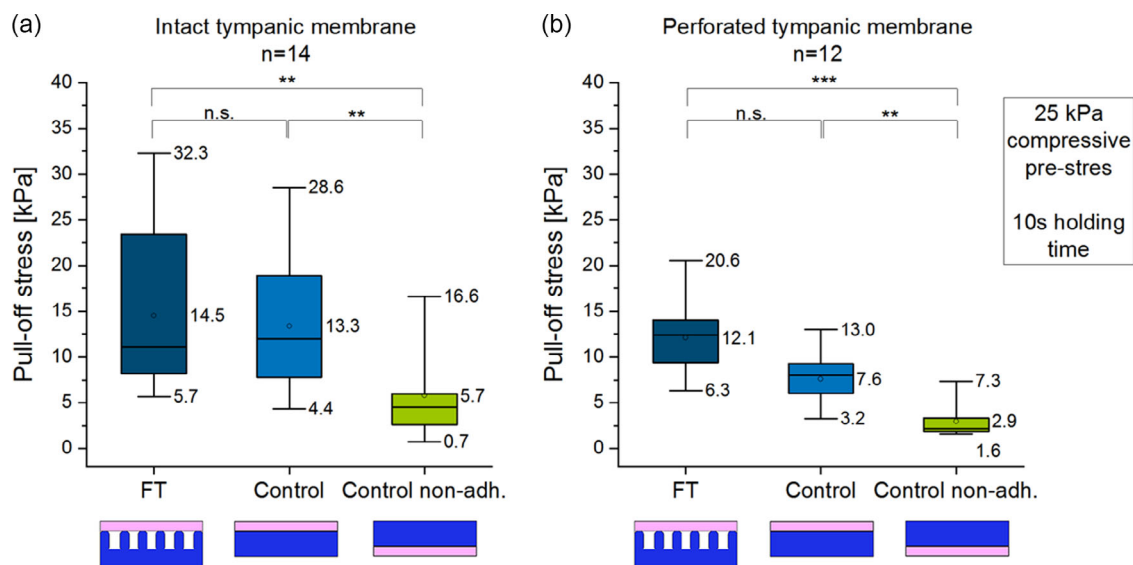


**Figure 5.** Pull-off stress for a) intact and b) perforated explanted TMs. Samples were film-terminated microstructures (FT, dark blue boxes) and unstructured control films with their adhesive side (control, light blue boxes) and their nonadhesive (nonadh., green boxes) side in contact. In the box and whisker plots, each box represents the range from the first quartile to the third quartile. The median is indicated by a line inside the box, the mean is indicated by a dot. The whiskers represent the ranges from the minimum to the maximum value of each group. Mean, minimum, and maximum values are also labeled with their values beside the boxes. Number *n* indicates independent measurements for a) *n* = 14, b) *n* = 12. *p*-Values are calculated using Kruskal–Wallis test followed by Dunn's test posthoc analysis for pairwise comparisons. \*\* indicates *p* < 0.01. \*\*\* indicates *p* < 0.001; n.s. = nonsignificant.

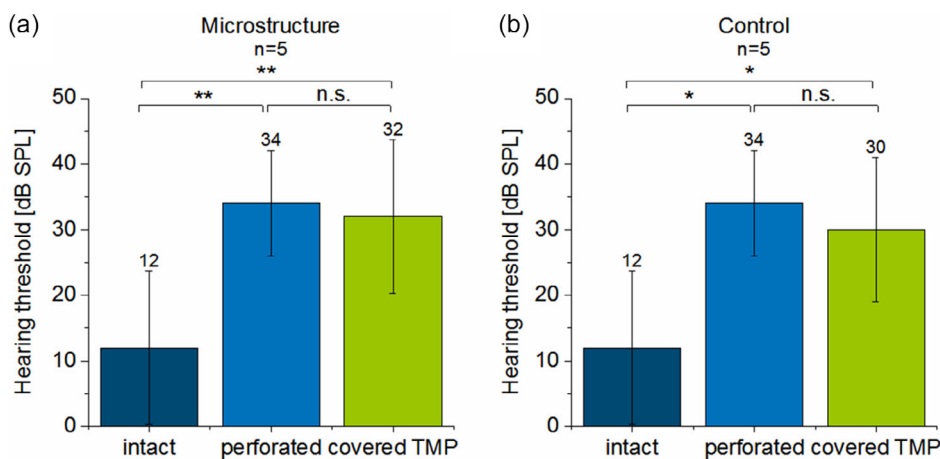


**Figure 6.** Analysis of the effects of perforation and covering of the TMP with a) microstructured or b) control patches on the hearing threshold, recorded by click–ABR in contrast to intact condition. The hearing threshold significantly increased after perforation from 12 to 34 dB SPL in both cases. a) After applying microstructured patches, the threshold decreased non-significantly to 32 dB SPL. b) After applying control patches, the threshold decreased non-significantly to 30 dB SPL. The data are presented as mean ± SD. The mean values are labeled above each graph, *n* = 5, *p*-values are calculated using one-way ANOVA with repeated measures followed by Bonferroni-test for pairwise comparison. \* indicates *p* < 0.05. \*\* indicates *p* < 0.01; n.s. = nonsignificant.

of the TM (Figure S1, Supporting Information). In all cases, the DPOAE signals were significantly reduced after patch application, especially for the coarser, more massive patches. When applied on the perforated membrane (Figure S2, Supporting Information), the coarser patches had no significant effect on the hearing function in comparison with the perforated condition.

From the surgeon's perspective, handling and application of the microstructured patches was more precise than for the controls, possibly because the pressure was more easily distributed

through the more compliant structure onto the thin TM. In addition, the microstructure adhered less to the thin forceps allowing easier adjustments of its position.

### 3. Discussion

In an attempt to improve current therapeutic strategies for surgical interventions on ruptured tympanic membranes, we

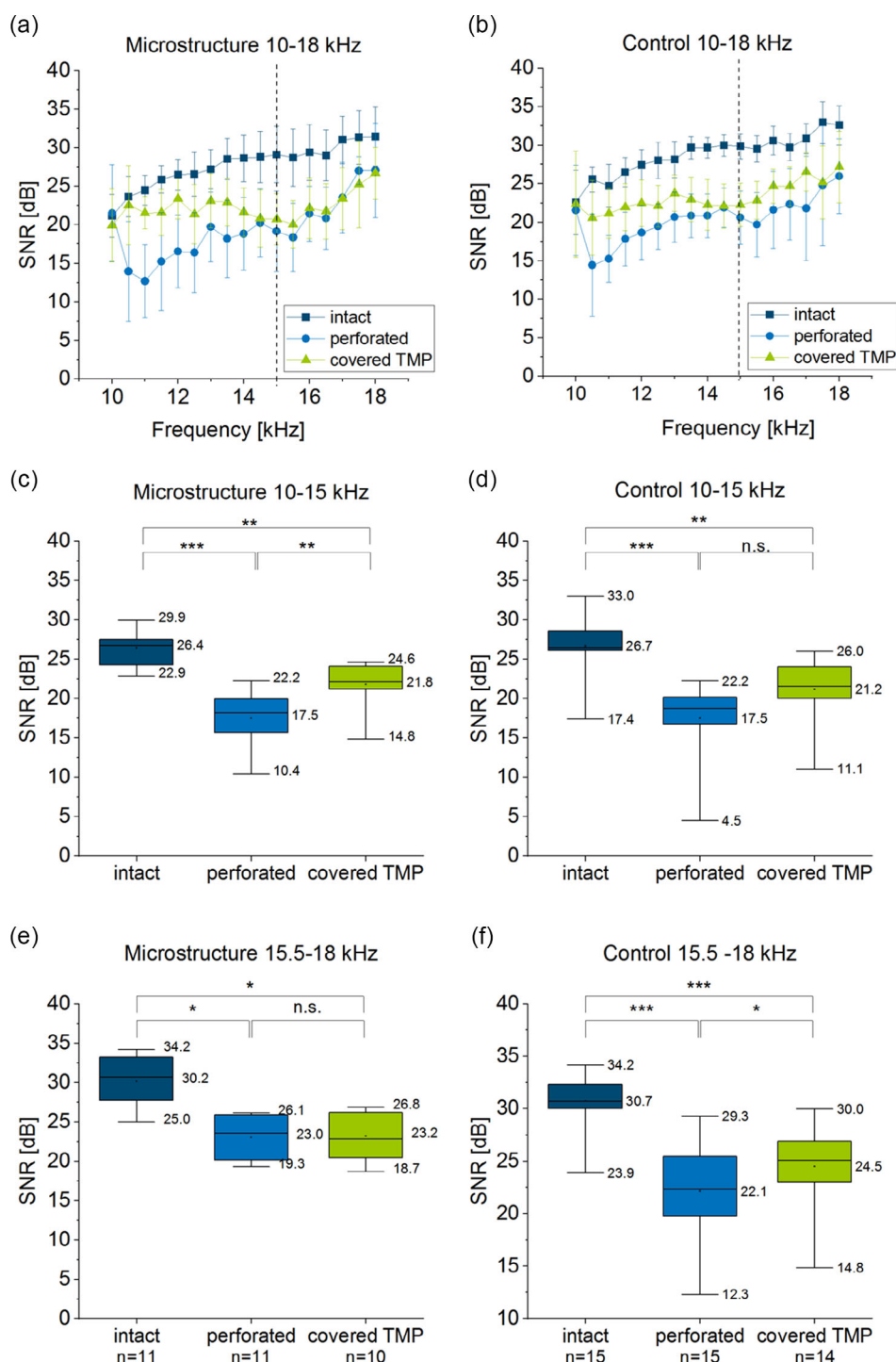


**Figure 7.** Hearing function in intact, perforated, and patched condition as measured by DPOAE. DPOAEs after treatment with microstructured patches (a, green data) showed an increase in the lower-frequency range, whereas the control (b) enhanced all frequencies compared with the perforated condition. c,d) Averaged SNRs point to a significant increase in DPOAE signals after patching compared with the untreated perforated TM between 10 and 15 kHz using the microstructure patches (c). d) Averaged SNRs were not significantly enhanced after applying control patches. e,f) Averaged SNRs in between 15.5 and 18 kHz. e) Microstructure patches led to a nonsignificant increase in SNRs, whereas in this frequency range, f) the application of control patches led to a significant increase in SNRs. Data are represented in a,b) as mean  $\pm$  SD. In the box and whisker plots, in c–f) each box represents the range from the first quartile to the third quartile. The median is indicated by a line inside the box, the mean is indicated by a dot. The whiskers represent the ranges from the minimum to the maximum value of each group. Mean, minimum, and maximum values are also labeled with their values beside the boxes. In c,f),  $p$ -values are calculated using ANOVA with repeated measures with Bonferroni test for pairwise comparisons and in e,d) with a Friedman–ANOVA with Dunn’s test for pairwise comparisons. \* indicates  $p < 0.05$ , \*\* indicates  $p < 0.01$ , and \*\*\* indicates  $p < 0.001$ , n.s. = nonsignificant. The number of replicates is indicated below the plots in e,f.

investigated a novel silicone microstructured patch in experiments with artificial surfaces and in a mouse model. Three main aspects will be discussed in turn: roughness of the tympanic membrane, adhesive properties of the patch, and its effect on hearing performance.

### 3.1. Roughness Characterization of the Murine TM

Aiming the development of an adhesive patch for application at the eardrum and considering the roughness as the first challenging factor against adhesion due to reduction of contact between two surfaces, we first evaluated this parameter of the tympanic membrane and the proposed model surface.

The height profiles in Figure 2b,c are, to our knowledge, the first reported roughness data for tympanic membranes of mice. The eardrum replicas are believed to closely match the conditions of the real murine membrane although slight material shrinkage could have affected the results.<sup>[14]</sup> The data showed relatively smooth surfaces for the TM ( $R_a \approx 0.14 \mu\text{m}$  and  $R_z \approx 1.18 \mu\text{m}$ ), in comparison, for example, to the roughness of human skin reported in literature ( $R_a \approx 13\text{--}16 \mu\text{m}$  and  $R_z \approx 61\text{--}71 \mu\text{m}$ ).<sup>[10]</sup> It should however be noted that singular values of  $R_a$  or  $R_z$  are insufficient descriptors of complex rough surfaces; a full analysis of the surface roughness using a power spectrum, as was carried out for skin, e.g., by Kovalev et al., was beyond the scope of this article.<sup>[41]</sup>

As a model surface, we chose an epoxy replica of frosted glass, whose roughness profile was comparable but did not fully match that of the eardrum. The epoxy exhibited a more homogeneously distributed roughness than the tympanic membrane, with higher  $R_z$  roughness values.

### 3.2. Adhesion Properties of the Patches

Against the epoxy model surface, our film-terminated microstructures demonstrated, for all tested parameters, higher adhesion in comparison with unstructured controls (Figure 3). This very likely reflects the previously studied crack trapping mechanism,<sup>[15,16]</sup> possibly in combination with the reduced effective modulus which facilitates adaptation to surface roughness. The advantage of the microstructure was especially pronounced (almost by a factor 2) for the smaller prestress value (11 kPa). For the larger prestress (23 kPa), on the other hand, the improvement was only about 27%. A possible explanation is the very soft top layer, which adapts to the surface topography leading to complete contact and a maximum pull-off stress when the prestress is sufficiently high.<sup>[17,42]</sup> The high adhesion for small prestress could be beneficial for future application in humans, as smaller forces exerted by the surgeon will lower the likelihood of damaging the TM.

As a next step, we evaluated the adhesion of the films on explanted tympanic membranes of mice as self-adhesion is an essential aspect for our novel designed films for eardrum perforation treatment. This characteristic gives them the advantage over the commercially available, nonadherent films, to not require packing of the outer ear canal with the consequent additional hearing impairment during the healing time. This experiment was carried out, to our best knowledge, for the first time in

the literature and required the design of a dedicated ex vivo measurement set-up. First, it was found that the adhesion values were generally lower for the perforated TM compared with the intact TM, presumably due to the reduction in actual contact area. An additional effect could be the reduced tension of the pars tensa (PT) after perforation, which would lead to a less defined contact and make the countersurface more compliant.<sup>[43]</sup>

Second, the adhesion performances of the microstructure and the control were very similar, the difference was not statistically significant for both the intact and the perforated condition.

A third observation is the generally lower adhesion to the eardrum than to the epoxy model surface. This is not surprising as the two substrate materials differ greatly in elastic modulus and geometric complexity (i.e., the concave curvature of the eardrum versus a nominally flat epoxy surface). A related aspect was that the two test setups used differed in stiffness. Still our approach follows common practice in standardized testing of medical adhesives, where adhesion is measured against steel substrates and empirical correlations to skin adhesion are assumed.<sup>[44,45]</sup>

In more quantitative terms, the top layer thickness necessary to accommodate the roughness characterized by  $R_z$  can be estimated. Following Davis et al.<sup>[46]</sup> and Fischer et al.,<sup>[14]</sup> adhesion will be insensitive to roughness above a critical film thickness given approximately by

$$h_{\text{crit}} \approx R_z^2 \cdot \frac{E_{\text{eff}}}{W_{\text{ad}}} \quad (1)$$

where  $E_{\text{eff}}$  is the effective modulus and  $W_{\text{ad}}$  the work of adhesion, assumed to be  $50 \text{ mJ m}^{-2}$ . For a film made of MG7-1010 with a Young's modulus of  $250 \text{ kPa}$ <sup>[47]</sup> on the tympanic membrane ( $R_z = 1.18 \mu\text{m}$ ),  $h_{\text{crit}} \approx 7 \mu\text{m}$ , which is well below the thickness of the top layer ( $\approx 25 \mu\text{m}$ ). In contrast, for the rougher epoxy substrate,  $h_{\text{crit}} \approx 32 \mu\text{m}$ , which is close to the top layer thickness. These results indicate that the adhesion on the epoxy substrates must benefit from the compliance of the underlying microstructure, whereas that on the explanted TM is solely associated with accommodation by the soft top layer, as in the control sample. Although the present results for microstructured patches did not confirm improved adhesion to murine eardrums, microstructures are expected to benefit in clinical applications where adhesion must be ensured to rougher human TMs. Work along these lines is currently in progress. In addition to advantageous adhesion on the rougher TM, the microstructure could even be further optimized by varying the top layer and the pillars dimensions,<sup>[17,47]</sup> allowing for a tunable and more personalized design of the patches, according to the patient's needs. Thereby, the adhesion could be easily adapted to the specific pathological findings. For example, larger or longer persistent perforations might need stronger adhesion to stay attached longer, in comparison with small acute perforations that heal faster. Another important argument in favor of our microstructured patches is the experience gained in the animal experiments that indicated that these patches proved to be easier to apply to the murine TM. The microstructures allowed for better gripping, were easier to handle and less prone to rolling-up. This can be explained by comparing the bending stiffness of both samples (calculations shown in Supporting Information). The calculated value of bending stiffness is almost 2.3 times higher for the microstructure than



the control sample (see Figure S3 and Section 1, Supporting Information). Also, the more even distribution of the compressive prestress improves the integrity of the remaining TM and ensures homogeneous adhesion without causing macroscopic damage of the sensitive membrane during removal. The film-terminated design offers the advantage, over bare micropillars, of proper sealing of the perforation especially along the perforation margins. This restores, at least partially, the acoustic and protective properties of the TM.

One further advantage of the film-terminated microstructures could be the insertion of inflammation- and infection-suppressing agents, e.g., cortisone or antibiotics between the pillar portions. The porosity of the top layer would allow diffusion through the material directly to the desired target location. This could result in an engineered release system allowing drug application over a predetermined time.<sup>[48,49]</sup>

### 3.3. Functional Effects on Hearing Ability

To our knowledge, we report here for the first time that appropriately designed adhesive patches have a positive impact on the hearing ability during the healing phase. DPOAE signals were significantly improved immediately following application of microstructured or control patches (Figure 7). The hearing threshold using click-ABR remained largely unaffected (Figure 6) due to the characteristics of click tones used in ABRs containing a wide range of frequencies applied simultaneously.

The frequency-specific analysis of DPOAE demonstrated that microstructured patches enhanced especially the lower frequencies (up to 15 kHz), whereas control patches improved the higher frequency range (between 15.5 and 18 kHz) (Figure 7). After translation to the much thicker human eardrum (thickness  $\approx 120\ \mu\text{m}$  compared with  $\approx 5\ \mu\text{m}$  for the mouse), these damping effects are expected to be much reduced in the final clinical application. Overall, the results will need to be newly evaluated in humans due to different dimensions of the eardrum.

The patches cannot fully restore the function of the damaged eardrum in the mouse model. This is very likely due to the added mass, which influences the acoustic impedance and dampens sound conduction. This effect was proven by the reduction in DPOAE levels after applying patches to intact TMs (Figure S1, Supporting Information). In evaluating these effects, the correlation of DPOAE signals with the state of the TM requires further discussion. In general, the signal level is strongly dependent on the anterograde and retrograde middle-ear transmission and is hence influenced by mechanical changes in the outer ear and middle ear, such as increased mass or stiffness. As a result, the middle ear constitution influences the DPOAE quality twice, by affecting the incoming tones in the inward-direction and the returning DPOAE signals in the outward direction.<sup>[32]</sup> DPOAEs are therefore valuable in detecting not only sensorineural but also conductive hearing loss<sup>[30]</sup> and are routinely used in clinical diagnosis.<sup>[50–52]</sup> In their study on gerbils, Dong et al.<sup>[32]</sup> analyzed the effects of TM perforations and altered middle ear transmission conditions on the generation of DPOAEs. DPOAEs were found to be measurable up to perforation sizes covering about half the tympanic membrane. DPOAE thresholds were not totally restored to normal after 4 weeks of incubation, especially at

higher frequencies ( $>10\ \text{kHz}$ ). The fact that DPOAE signals did not totally recover even after closure of the TM perforation was ascribed to an incompletely restored middle ear transmission.

The immediate improvement of the auditory function in mice, as suggested by our study, would be advantageous for the treatment of patients, who would also benefit from a free ear canal during the healing phase. According to most studies of the healing time of TMs, we expect a retention time of more than 4 weeks of the patch on the perforated membrane.<sup>[53–55]</sup> To the best of our knowledge, most studies on TMP treatment use nonadhesive materials that require the packing procedure of the outer ear canal to keep the patch in position. In the study of Farhadi et al.,<sup>[37]</sup> collagen-covered PDMS patches applied to longstanding, small perforations in ten patients had an overall success rate of 70% after 1 month. These patches had to be fixated by gel foam, which led to an inevitable conductive hearing loss. Park et al. reported about the use of Steri-Strip patching, an adhesive material using for wound closure, in comparison with paper patch and spontaneous closure and reported decreased need for repeated patching procedures in the Steri-Strip group. On the other hand, in the Steri-Strip group, significantly increased rates of otorrhea occurred.<sup>[56]</sup> Further studies on adhesive patching, published by Aslan et al. 2011, reported on an immediate hearing improvement after patching with Steri-Strips except in the patients with chronic perforations.<sup>[57]</sup> Self-adhesive silicone elastomers offer the advantage to be applied and fixed without the need of chemical glues, as e.g., acrylic adhesives used in Steri-Strips. Combined with the positive effects on the hearing performance after patching, silicone elastomers offer a minimally invasive, cost-effective, time saving, and easy to use technique for closing TMPs.

For future medical treatments of TMPs, cell growth on our adhesives is an important factor. In previous studies, we successfully demonstrated that cells spread in functionalized MG7-9800,<sup>[39,58]</sup> which is a similar soft skin adhesive as the MG7-1010 used in our study. However, these studies have to be repeated for the current material before considering clinical trials. Although less quantifiable, the surgeon's experience with the microstructured patches will be an important factor in their clinical success. The generally positive perception with regard to ease of handling, coupled with the potential benefits to the patient during and after the healing period, enhances the chances of a successful translation of these novel microstructured patches into clinical practice.

## 4. Conclusions

We present, for the first time, the design and fabrication of microstructured, film-terminated silicone patches for application on tympanic membrane perforations. These structures were tested first on relatively rough artificial rigid surfaces, where they demonstrated higher pull-off stresses compared with the unstructured controls. The adhesion of both types of patches, tested on murine explanted tympanic membranes using a customized setup, was similar for both samples. We foresee, however, a positive effect of microstructured patches on human tympanic membranes, which exhibit greater roughness. In

addition, through the continuous top layer, the patches allow proper sealing of the perforation and may avoid the entrance of pathogens into the middle ear. In a living animal model, the hearing function, investigated by DPOAE signals, was partially restored immediately after patch application. The microstructured patches allowed for better gripping by the surgeon and were easier to handle. They offer great potential for future treatment of patients suffering from a TMP. Further studies of these novel silicone patches, regarding their effects on healing and long-time behavior, are underway to ensure safe and effective clinical treatment of TMPs.

## 5. Experimental Section

**Fabrication of Film-Terminated and Control Samples:** A new film-terminated microstructure was developed using pillars of  $\approx 20\ \mu\text{m}$  diameter and  $60\ \mu\text{m}$  height (aspect ratio 3), with hexagonal configuration and interpillar distance equal to their diameter. The pillar fabrication process consisted of two replication steps. First, a master structure with a  $0.5 \times 0.5\ \text{cm}^2$  pillar array was printed on a  $2.5 \times 2.5\ \text{cm}^2$  silicon wafer using a methacrylate-based resin (Nanoscribe IP-Q Resin) by two-photon lithography (Photonic Professional GT2, Nanoscribe, Eggenstein–Leopoldshafen, Germany). The master structure was cleaned with isopropanol and gently dried using nitrogen flow. The surface of the master structure was coated with (tridecafluoro-1,1,2,2-tetrahydrooctyl) trichlorosilane (AB111444, ABCR, 97%) upon activation in an air plasma (Atto low pressure plasma system, Electronic Diener, Ebhausen, Germany) for 5 min. Coating occurred via vapor deposition in reduced pressure of about 3 mbar for 15 min. A mold (negative) was thereafter replicated from the master by pouring PDMS (Elastomer kit Sylgard 184, Dow Silicones, Midland, MI, USA) onto the microstructure placed in a Petri dish. After curing for 1 h at  $95^\circ\text{C}$ , the mold was gently peeled and silanized using the same process as described earlier. Sylgard 184 was poured on the mold and degassed for 5 min to properly fill the cavities. Then, the excessive polymer was removed by spinning the mold at 1000 rpm for 120 s (Spin coater Laurell WS 650 MZ-23NPPB, North Wales, Pennsylvania, USA). This resulted in a homogeneous backing layer, the base for the pillars. After curing at  $95^\circ\text{C}$  for 1 h, the pillar array was gently removed from the mold and placed on a polyethyleneterephthalat (PET) film to stabilize the microstructure and facilitate handling. For film-termination, first a thin MG7-1010 (Dow Silicones, Midland, Michigan, USA) film was prepared on a fluorosilicone release liner (Siliconature, SILFLU S 75 M 1R88002 clear) at 7000 rpm for 120 s and subsequently cured at  $95^\circ\text{C}$  for 1 h. On top of this film, a second layer of MG7-1010 was prepared, again using 7000 rpm. The microstructure was placed upside down onto the uncured film and subsequently cured. Upon peeling the entire structure from the release liner, the film-terminated microstructures were used without further treatments. It is to be noted that MG 7-1010 is a certified medical product. In accordance with the safety data sheet, skin absorption of hazardous substances is unlikely even after long-term exposure to skin.

The unstructured samples (to be referred to as “control sample”) were prepared by first fabricating a Sylgard film on a PET film using a doctor blade (AFA-IV, MTI Corporation, Richmond, CA, USA). The thickness of the Sylgard layer was chosen according to the amount of Sylgard used for the microstructured specimen to match the mass of the sample. The soft skin adhesive layer was added with the same procedure as the film-termination described earlier. All specimen dimensions were measured using an optical microscope (Eclipse LV100ND, Nikon, Tokyo, Japan) and a scanning electron microscope (FEI Quanta 400 ESEM, Thermo Fisher, USA). For the latter, specimens were sputter-coated with gold and analyzed under high vacuum, below  $3 \times 10^{-2}\ \text{Pa}$ , 7 kV voltage and a secondary electron detector.

**Roughness of Model Surfaces and Tympanic Membranes:** The roughness of the substrate surfaces made from epoxy was measured using a confocal microscope (MarSurf CM explorer, Mahr, Göttingen, Germany). Measurements were carried out at three positions using a  $50\times$  objective. The roughness of the murine TM was indirectly determined by measuring silicone replicas prepared prior to the ex vivo adhesion measurements (see Section 2.4). In total, 14 replicas of seven eardrums were measured, each of them at three different positions of the PT, using a  $50\times$  objective. The surface analysis was carried out using the software “Marsurf MFM Extended” on a surface of dimensions  $320 \times 320\ \mu\text{m}^2$ . The raw data were fitted with a Gaussian filter having a cut-off length of  $2.5\ \mu\text{m}$ , a seventh-order polynomial and a cut-off length of  $250\ \mu\text{m}$ .

**Adhesion Measurements:** Tack tests were carried out using a custom-built adhesion testing device.<sup>[58,59]</sup> Normal forces were recorded using a 0.25 N load cell (ME-Meßsysteme GmbH, Hennigsdorf, Germany). The surface used for adhesion measurements was the flat face of a cylinder made from epoxy resin, replicating a frosted glass slide (Marienfeld, Lauda Königshofen, Germany). For details see the study by Fischer et al.<sup>[14]</sup>

The measurements were carried out by approaching the sample to the substrate surface at a rate of  $30\ \text{m s}^{-1}$  until a compressive preload of 30 or 60 mN was reached. The sample was held in contact with the surface for 10 s, and then retracted with a velocity of  $10\ \text{m s}^{-1}$  until pull-off occurred. Each sample was measured at three different independent positions (error bars represent standard deviation [SD]). Displacements recorded were corrected for the system compliance  $C = 0.13\ \mu\text{m mN}^{-1}$ .<sup>[14]</sup> The maximum pull-off stress was calculated by dividing the force values by the nominal contact area of  $2.6\ \text{mm}^2$ .<sup>[14]</sup>

**Animal Experiments:** All animal experiments were carried out under anesthesia (auditory measurement) or ex vivo on freshly explanted TM specimens. All experiments were conducted according to the German Animal Welfare Law following the EU directive 2016/63/EU for animal experiments by qualified persons. The Animal Welfare Officer of the Saarland University was informed in advance and the euthanasia methods were fully appropriate. We ensured the minimizing of discomfort, stress, and pain during the experiments using proper anesthesia and analgesics. Furthermore, the animals were kept hydrated and the body temperature was maintained using an electric heating pad. For anesthesia, a mixture of ketamine-hydrochloride ( $80\ \text{mg kg}^{-1}$  body weight [BW] Ursotamin, Serumwerk Bernburg, Germany) and xylazine-hydrochloride ( $10\ \text{mg kg}^{-1}$  BW; Xylazin, Serumwerk Bernburg, Germany) was injected intraperitoneally with an injection volume of  $10\ \text{mL kg}^{-1}$  BW. The anesthesia was maintained by injecting one-third of the initial dose intraperitoneally, typically in 30–40 min intervals. For terminal experiments, the animals were sacrificed in deep anesthesia.

**Surface Roughness Determination and Tack Tests on Explanted Mouse TM:** To analyze the adhesion of film-terminated microstructures and the non-structured control films on the murine TM, tack tests were carried out on explanted TMs. These experiments were conducted in accordance with EU directive 2016/63/EU for animal experiments as acute experiments. The Animal Welfare Officer was informed about them and all experiments were conducted by qualified persons. The preparation of mouse tympanic membranes was carried out as described previously.<sup>[39]</sup> For the preparation of the specimens, the outer ear canal was trimmed down to the bony part. The bony portion of the ear canal that covered a major part of the eardrum was carefully removed by clipping, keeping enough distance to the eardrum to ensure that the TM would not be affected by the preparation. The petrosal bone, containing the tympanic capsule with the eardrum, the middle ear ossicular chain, and the cochlea, was then carefully detached from the skull bone and mounted onto a glass substrate. For the assembly, a two-component methyl methacrylate (Technovit 4004, Kulzer Technik, Hanau, Germany) was used, while ensuring free oscillation of the eardrum. After curing, the glass substrate was mounted to a sample holder. Prior to the adhesion measurements, a negative replica of the membrane was prepared using a two-component silicone (R&S Turboflex.0122 996, CFPM, Tremblay-en-France, France). The components were mixed 1:1 and carefully applied onto the TM, ensuring that the whole membrane was covered, especially including the area under the residual bony parts of the outer ear canal. In addition, it was verified

that no residual air bubbles remained. The molding material was cured at room temperature for  $\approx 5$  min and then gently removed. This negative mold was used to analyze the surface roughness of the TM.

The adhesion tests for real tissue were carried out with a custom-made setup. Adhesive samples were cut under visual control into circular pieces with a diameter of  $\approx 1$  mm using a biopsy punch and carefully fixed on the customized applicator using double-sided tape. This applicator was connected to the load cell (ME-Meßsysteme GmbH, Hennigsdorf, Germany) of our setup (see Section 3.4, Figure 4a). It was aligned to the sample holder under visual control to ensure positioning of the adhesive film parallel to the tympanic membrane surface (Figure 4b). The applicator containing the film was moved toward the TM at a constant speed of  $0.03 \text{ mm s}^{-1}$ , until a compressive stress of  $\approx 25 \text{ kPa}$  was reached, held for 10 s and then pulled off at  $0.1 \text{ mm s}^{-1}$  until total detachment (Figure 4c). The adhesive force was recorded and analyzed. In total, five tympanic membranes were used for the adhesion measurements, in intact and perforated conditions. Seven independently prepared sets of film-terminated and control patches were tested. As further validation, the control patches were tested on both the adhesive and nonadhesive sides. The experiments were carried out in a random sequence.

**Electrophysiological Measurement of Auditory Function by ABRs and DPOAEs Recordings:** The auditory recordings were carried out in a soundproofed room (camera silent) on a preparation table isolated against vibrations. ABR recordings are a standard method to assess auditory function in both clinical and research setups in humans and laboratory animals.<sup>[60,61]</sup> The click ABRs were carried out as described previously<sup>[62,63]</sup> to detect the auditory threshold in intact and perforated conditions as well as after applying a patch on the perforation. The auditory threshold was characterized as the lowest intensity where the Jewett's wave complex consisting of five positive waves was identifiable.<sup>[61,64]</sup>

DPOAEs were measured with a DPOAE probe, which is used in clinical setup (UGD, Otodynamics, Hatfield, UK) as described previously.<sup>[65]</sup> DPOAE signals were elicited by two pure-tone stimuli (with frequency  $f_1$  and  $f_2$ ) on two different speakers with a level of  $L_1 = 55 \text{ dB SPL}$ ,  $L_2 = 45 \text{ dB SPL}$ , and  $f_2/f_1 = 1.22$ , as described by Engel et al.<sup>[66]</sup> Despite a high number of emitted distortion products, current clinical DPOAE devices only make use of the emitted signal at the frequency component  $2f_2 - f_1$  as a diagnostic parameter. The DPOAE amplitudes were measured between 10 and 18 kHz using 0.5 kHz steps followed by averaging and displayed as signal-to-noise ratio (SNR).<sup>[65,67,68]</sup> DPOAE measurements were carried out in three different conditions: 1) intact TM, 2) perforated TM, and 3) perforated TM with a patch in the same animal.

PDMS patches processed as described earlier were cut manually to  $\approx 1$  mm diameter under microscope control. A perforation was induced in the posterior quadrant of the TM using a suction tube of 1.3 mm outside diameter (KARL STORZ SE & Co. KG, Tuttlingen, Germany). The DPOAEs were recorded intact, with perforation and with a patch covering the perforation. Upon completion of the set of measurements, the animal was sacrificed under deep anesthesia, the petrosal bones were explanted and the size of the TM perforation was analyzed using a microscope (MZ10F, Leica, Wetzlar, Germany) and the respective microscopy software (LASX, Leica, Wetzlar, Germany).

**Statistical Analysis:** Continuous variables in bar graphs are represented as mean  $\pm$  SD. In the box and whisker plots, each box represents the range from the first quartile to the third quartile. The median is indicated by a line inside the box, the mean is indicated by a dot. The whiskers represent the ranges from the minimum to the maximum value of each group. The Shapiro-Wilk test was applied to verify the normal distribution of the data. Variance homogeneity was tested by a Levene's test.

For the analysis of adhesive strength analyzed by tack tests on epoxy substrates, the pull-off stresses were compared via a two-sided *t*-test. For the analysis of the DPOAEs and the pull-off stresses *ex vivo*, we used a one-way analysis of variance (ANOVA). For the analysis of the *ex vivo* pull-off stress, the groups were independent, so ANOVA was carried out for normally distributed data. If normal distribution was not given, the Kruskal-Wallis test was used as a nonparametric test with a Dunn's test as posthoc analysis for pairwise comparison. The Bonferroni test was used in case of variance equality for pairwise

comparisons. The results of the DPOAEs and Click-ABR thresholds were analyzed as paired samples. For this purpose, we carried out ANOVA with repeated measures for normally distributed data followed by Levene's test for variance homogeneity and Bonferroni test for pairwise comparison. When normal distribution or variance equality was not given, the DPOAE data were analyzed by Friedman-ANOVA followed by a posthoc analysis with a Dunn's test for pairwise comparisons. In all cases, significance was defined as  $p \leq 0.05$ . For statistical analysis, OriginPro 2020 software was used (OriginLab Corp., North Hampton, USA).

## Supporting Information

Supporting Information is available from the Wiley Online Library or from the author.

## Acknowledgements

The authors acknowledge Joachim Blau for technical support and for designing the *ex vivo* measurement setup. Julian Weiß is acknowledged for confocal microscopy measurements and Dr. Lena Barnefske for the microfabrication of the master structures. Dr. Xuan Zhang is thanked for the support in mechanical calculations and Angela Rutz, for her laboratory assistance. The authors thank Biesterfeld Spezialchemie GmbH (Hamburg, Germany) for providing the polymers and Isaac Ayala Design for the design of the schematic TM graphic shown in Figure 2. The research leading to these results has received funding from the European Research Council under the European Union's HORIZON2020-EU.1.1 program/ ERC PoC Grant Agreement No. 842 613, Advanced Grant "Stick2Heal" to E.A.

## Conflict of Interest

The authors declare no conflict of interest.

## Author Contributions

G.M.L. and K.S. contributed equally to this work. Conceptualization G.M.L., K.S., G.I.W., K.K., E.A.; Roughness and adhesion investigation G.M.L.; *Ex-situ* adhesion investigation G.M.L., K.S., K.K.; Hearing investigation K.S., K.K.; Statistical analysis K.S.; Writing – original draft: G.M.L., K.S. Writing – Review and editing: G.M.L., K.S., G.I.W., D.H., R.H., K.K., B.S., E.A.

## Data Availability Statement

Research data are not shared.

## Keywords

silicone patches, microstructured adhesives, tympanic membrane perforations, distortion product otoacoustic emissions

Received: May 12, 2021

Revised: June 1, 2021

Published online: July 31, 2021

[1] E. Arzt, H. Quan, R. M. McMeeking, R. Hensel, *Prog. Mater. Sci.* **2021**, 120, 100823.

[2] R. Hensel, K. Moh, E. Arzt, *Adv. Funct. Mater.* **2018**, 28, 1800865.

- [3] J. S. Kaiser, M. Kamperman, E. J. de Souza, B. Schick, E. Arzt, *Int. J. Artif. Organs* **2011**, 34, 180.
- [4] M. K. Kwak, C. Pang, H. E. Jeong, H. N. Kim, H. Yoon, H. S. Jung, K. Y. Suh, *Adv. Funct. Mater.* **2011**, 21, 3606.
- [5] D. M. Drotlef, M. Amjadi, M. Yunusa, M. Sitti, *Adv. Mater.* **2017**, 29, 1.
- [6] E. Arzt, S. Gorb, R. Spolenak, *Proc. Natl. Acad. Sci. U. S. A* **2003**, 100, 10603.
- [7] A. Del Campo, C. Greiner, I. Álvarez, E. Arzt, *Adv. Mater.* **2007**, 19, 1973.
- [8] S. C. L. Fischer, E. Arzt, R. Hensel, *ACS Appl. Mater. Interfaces* **2017**, 9, 1036.
- [9] V. Tinnemann, L. Hernández, S. C. L. Fischer, E. Arzt, R. Bennewitz, R. Hensel, *Adv. Funct. Mater.* **2019**, 29, 1807713.
- [10] C. Trojahn, M. Schario, G. Dobos, U. Blume-Peytavi, J. Kottner, *Ski. Res. Technol.* **2015**, 21, 54.
- [11] R. Maiti, L. C. Gerhardt, Z. S. Lee, R. A. Byers, D. Woods, J. A. Sanz-Herrera, S. E. Franklin, R. Lewis, S. J. Matcher, M. J. Carré, *J. Mech. Behav. Biomed. Mater.* **2016**, 62, 556.
- [12] D. Fuller, K. N. G. Tabor, *Proc. R. Soc. London. A. Math. Phys. Sci.* **1975**, 345, 327.
- [13] V. Barreau, R. Hensel, N. K. Guimard, A. Ghatak, R. M. McMeeking, E. Arzt, *Adv. Funct. Mater.* **2016**, 26, 4687.
- [14] S. C. L. Fischer, S. Boyadzhieva, R. Hensel, K. Kruttwig, E. Arzt, *J. Mech. Behav. Biomed. Mater.* **2018**, 80, 303.
- [15] N. J. Glassmaker, A. Jagota, C.-Y. Hui, W. L. Noderer, M. K. Chaudhury, *Proc. Natl. Acad. Sci.* **2007**, 104, 10786.
- [16] W. L. Noderer, L. Shen, S. Vajpayee, N. J. Glassmaker, A. Jagota, C. Y. Hui, *Proc. R. Soc. A* **2007**, 2631.
- [17] Z. He, N. M. Moyle, C. Y. Hui, B. Levrard, A. Jagota, *Tribol. Lett.* **2017**, 65, 1.
- [18] H. Shahsavan, D. Arunbabu, B. Zhao, *Macromol. Mater. Eng.* **2012**, 297, 743.
- [19] H. Shahsavan, B. Zhao, *Macromolecules* **2014**, 47, 353.
- [20] P. Hong, M. Bance, P. F. Gratzner, *Int. J. Pediatr. Otorhinolaryngol.* **2013**, 77, 3.
- [21] E. Dursun, S. Dogru, A. Gungor, H. Cincik, E. Poyrazoglu, T. Ozdemir, *Otolaryngol. – Head Neck Surg.* **2008**, 138, 353.
- [22] I. Ghanad, M. D. Polanik, D. R. Trakimas, R. M. Knoll, M. Castillo-Bustamante, N. L. Black, E. D. Kozin, A. K. Remenschneider, *Laryngoscope* **2020**, 131, 392.
- [23] G. Berger, Y. Finkelstein, S. Avraham, M. Himmelfarb, *J. Laryngol. Otol.* **1997**, 111, 1137.
- [24] R. P. Mehta, J. J. Rosowski, S. E. Voss, E. O'Neil, S. N. Merchant, *Otol. Neurotol.* **2006**, 27, 136.
- [25] O. A. Sogebi, E. A. Oyewole, T. O. Mabifah, *Ghana Med. J.* **2018**, 52, 34.
- [26] L. Louw, *J. Laryngol. Otol.* **2010**, 124, 587.
- [27] P. L. Santa Maria, P. Gottlieb, C. Santa Maria, S. Kim, S. Puria, Y. P. Yang, *Tissue Eng. Part A* **2017**, 23, 436.
- [28] T. Janssen, H. P. Niedermeyer, W. Arnold, *ORL* **2006**, 68, 334.
- [29] F. Zhao, H. Wada, T. Koike, D. Stephens, *Clin. Otolaryngol.* **2000**, 25, 3.
- [30] A. I. Tlumak, P. R. Kileny, *Curr. Opin. Otolaryngol. Head Neck Surg.* **2001**, 9, 279.
- [31] H. W. LeBourgeois, V. K. Anand, J. R. McAuley, J. D. Dickman, O. Malphurs, *Ear, Nose Throat J.* **2000**, 79, 610.
- [32] W. Dong, G. Stomackin, X. Lin, G. K. Martin, T. T. Jung, *Hear. Res.* **2019**, 378, 3.
- [33] F. Zöllner, *J. Laryngol. Otol.* **1955**, 69, 637.
- [34] H. Wullstein, *Arch. für Ohren-, Nasen-, und Kehlkopfheilkd* **1952**, 422.
- [35] J. M. Hempel, A. Becker, J. Müller, E. Krause, A. Berghaus, T. Braun, *Otol. Neurotol.* **2012**, 33, 1357.
- [36] S. Branica, K. Dawidowsky, L. Kovač-Bilić, M. Bilić, *Croat. Med. J.* **2019**, 60, 503.
- [37] M. Farhadi, H. Mirzadeh, A. Solouk, A. Asghari, M. Jaleesi, H. Ghanbari, P. Yazdanifard, *J. Biomed. Mater. Res. A* **2011**, 100A, 549.
- [38] S. Boyadzhieva, S. C. L. Fischer, S. Lösch, A. Rutz, E. Arzt, K. Kruttwig, *J. Vis. Exp.* **2018**, 2018, 57573.
- [39] S. Boyadzhieva, K. Sorg, M. Danner, S. C. L. Fischer, R. Hensel, B. Schick, G. Wenzel, E. Arzt, K. Kruttwig, *Polymers* **2019**, 11, 942.
- [40] C. Creton, M. Ciccotti, *Reports Prog. Phys.* **2016**, 79, 46601.
- [41] A. E. Kovalev, K. Dening, B. N. J. Persson, S. N. Gorb, *Beilstein J. Nanotechnol.* **2014**, 5, 1341.
- [42] H. Shahsavan, B. Zhao, *Soft Matter* **2012**, 8, 8281.
- [43] L. Caminos, J. García-Manrique, A. Lima-Rodríguez, A. Gonzalez-Herrera, *Appl. Bionics Biomech.* **2018**, 2018, 1.
- [44] I. O. for S. ISO, *Self Adhesive Tapes – Determination of Peel Adhesion Properties*, **2007**.
- [45] I. O. for S. ISO, *Self Adhesive Tapes – Measurement of Peel Adhesion from Stainless Steel or from Its Own Backing*, **1997**.
- [46] C. S. Davis, D. Martina, C. Creton, A. Lindner, A. J. Crosby, *Langmuir* **2012**, 28, 14899.
- [47] J. M. Eubel, Design Und Herstellung Eines Haftsystem Zur Anwendung Auf Dem Trommelfell, Universität des Saarlandes, **2019**.
- [48] B. Mikolaszek, J. Kazlauske, A. Larsson, M. Sznitowska, *Polymers* **2020**, 12, 1520.
- [49] K. Yu, J. Hou, Z. Jin, K. Wu, S. Xu, N. Yang, Y. Shen, T. Tang, S. Guo, *J. Drug Deliv. Sci. Technol.* **2018**, 46, 173.
- [50] C. M. Blankenship, L. L. Hunter, D. H. Keefe, M. Patrick Feeney, D. K. Brown, A. McCune, D. F. Fitzpatrick, L. Lin, in *Ear Hear., Lippincott Williams And Wilkins, Philadelphia, PA* **2018**, pp. 1075–1090.
- [51] D. Colon, U. Verdugo-Raab, C. Alvarez, T. Steffens, S. Marcrum, S. Kolb, C. Herr, D. Twardella, *Noise Heal.* **2016**, 18, 288.
- [52] L. A. Ohlms, B. L. Lonsbury-Martin, G. K. Martin, *Otolaryngol. – Head Neck Surg.*, **1990**, 103, 52.
- [53] J. E. O. Amadasun, *J. Laryngol. Otol.* **2002**, 116, 181.
- [54] Z. Lou, Y. Wang, K. Su, *Eur. Arch. Oto-Rhino-Laryngol.* **2014**, 271, 2153.
- [55] I. Saliba, *Clin. Otolaryngol.* **2008**, 33, 610.
- [56] M. K. Park, K. H. Kim, J. D. Lee, B. D. Lee, *Otolaryngol. Head. Neck Surg.* **2011**, 145, 581.
- [57] G. Aslan, L. Uzun, *Oper. Tech. Otolaryngol. – Head Neck Surg.* **2011**, 22, 173.
- [58] S. C. L. Fischer, K. Kruttwig, V. Bandmann, R. Hensel, E. Arzt, *Macromol. Mater. Eng.* **2017**, 302, 1.
- [59] E. Kroner, J. Blau, E. Arzt, *Rev. Sci. Instrum.* **2012**, 83, 2.
- [60] J. F. Willott, *Curr. Protoc. Neurosci.* **2006**, 34, 8.21B.1.
- [61] L. Rüttiger, U. Zimmermann, M. Knipper, *Orl* **2017**, 79, 93.
- [62] K. Sorg, P. Stahn, L. Pillong, M. P. Hinsberger, L. Heimann, H.-J. Foth, B. Schick, G. I. Wenzel, *J. Biomed. Opt.* **2019**, 24, 1.
- [63] S. A. L. Schacht, P. Stahn, M. Hinsberger, B. Schick, G. I. Wenzel, *J. Biomed. Opt.* **2018**, 23, 1.
- [64] Q. Y. Zheng, K. R. Johnson, L. C. Erway, *Hear. Res.* **1999**, 130, 94.
- [65] D. J. Hecker, J. Lohscheller, C. A. Bader, W. Delb, B. Schick, J. Dlugaczky, *IEEE Trans. Biomed. Eng.* **2011**, 58, 2369.
- [66] J. Engel, C. Braig, L. Rüttiger, S. Kuhn, U. Zimmermann, N. Blin, M. Sausbier, H. Kalbacher, S. Münkner, K. Rohbock, P. Ruth, H. Winter, M. Knipper, *Neuroscience* **2006**, 143, 837.
- [67] T. Schimmang, J. Tan, M. Müller, U. Zimmermann, K. Rohbock, I. Köpschall, A. Limberger, L. Minichiello, M. Knipper, *Development* **2003**, 130, 4741.
- [68] B. Fell, S. Eckrich, K. Blum, T. Eckrich, D. Hecker, G. J. Obermair, S. Münkner, V. Flockerzi, B. Schick, J. Engel, *J. Neurosci.* **2016**, 36, 11024.